Modeling Particle Shape-Dependent Dynamics in Nanomedicine

Samar Shah[1], Yaling Liu[1*], Wenchuang Hu[2], Jinming Gao[3]

[1]Department of Mechanical and Aerospace Engineering
The University of Texas at Arlington, Arlington, Texas, 76019
[2]Department of Electrical Engineering
The University of Texas at Dallas, Richardson, TX 75080
[3]Department of Pharmacology, Harold C. Simmons Comprehensive Cancer Center,
University of Texas Southwestern Medical Center, Dallas, TX 75390

One of the major challenges in nanomedicine is to improve nanoparticle cell selectivity and adhesion efficiency through designing functionalized nanoparticles of controlled sizes, shapes, and material compositions. Recent data on cylindrically shaped filomicelles are beginning to show non-spherical particles remarkably improved the biological properties over spherical counterpart. Despite these exciting advances, non-spherical particles have not been widely used in nanomedicine applications due to the lack of fundamental understanding of shape effect on targeting efficiency. This paper intends to investigate the shape-dependent adhesion kinetics of non-spherical nanoparticles through computational modeling. The ligand-receptor binding kinetics is coupled with Brownian dynamics to study the dynamic process of nanorods tumbling, diffusion and adhesion under various vascular flow conditions. The influences of nanoparticle shape, ligand density, and shear rate on adhesion probability are studied. Nanorods are found to contact and adhere to the wall easier than their spherical counterparts under the same configuration due to the tumbling motion. Results from this study contribute to the fundamental understanding and knowledge on how particle shape affects the transport and targeting efficiency of nanocarriers, which will provide mechanistic insights on the design of shape-specific nanomedicine for targeted drug delivery applications.

Introduction

In recent years, nanoparticulate systems have been widely used for diagnostic imaging and targeted therapeutic applications.[1-9] Various nanoplatforms, including liposomes,[10,11] polymeric micelles,[12-14] quantum dots,[15,16] Au/Si/polymer shells,[17-19] and dentrimers[20-22] have been established with distinctive chemical compositions and biological properties. Extensive studies have elucidated the effects of particle *size* (mostly from spherical ones) on their clearance, circulation, extravasation, and distribution *in vivo*. However, the effects of particle *shape* on its fate are much less understood in nanomedicine. In nature, viruses have a variety of shapes from icosahedral to bullet/rod, yet the biological functions of shape are not clearly understood in relation to host infection and virus survival. Recently, synthetic non-spherical nanoparticles have shown significantly improved biological properties over the spherical counterparts. For example, cylindrically shaped filomicelles can effectively evade the non-specific uptake by the reticuloendothelial systems and persist in the circulation up to one week after intravenous injection (~10 times longer than the spheres).[23] Dai and coworkers reported that single-walled carbon nanotubes (SWNT, diameter 1-5 nm, length 100-300 nm) can enhance polyvalent targeting of surface-bound peptide to the tumor cells, leading to highly elevated particle accumulation (13% injected dose/g tissue as compared to 1-2% for spherical particles) in tumors[24]. Sailor and coworkers demonstrate improved tumor accumulation and retention of worm-shaped iron oxide nanoparticles that are encoded with F3 peptides over spherical counterparts[25]. Despite these exciting advances, the mechanistic understanding of shape functions in biological systems has been lacking.

The targeted delivery process by nanoparticles involves interplay of transport, hydrodynamic force, and multivalent interactions with targeted biosurfaces [26]. Due to the small size of nanoparticles and the dynamic nature of the transportation-deposition process, it is a very challenging task to explore this phenomenon experimentally. Theoretical works of nanoparticle deposition are limited to simple spherical or oblate shape for an ideal configuration and steady state condition.[27-29] Theoretical modeling of nanoparticle adhesion kinetics has focused mostly on spherical nanoparticles. It is only recently that non-spherical nanoparticle attracted some attention. For example, Decuzzi and Ferrari[27-29] have studied the margination of nanoparticle vectors in blood stream, where the nanoparticles diffusion in a Newtonian fluid was investigated. The same authors have also studied the adhesion probability of nanoparticles for an equilibrium configuration. In their work, the margination and adhesion process are studied separately. Only simple spherical or oblate-shaped nanoparticles are considered, leaving rod and disk shaped nanoparticles un-explored. A coupled model that links margination with adhesion kinetics and applicable to nanoparticle of various shapes is yet to be developed. Thus, characterization of this process for arbitrarily shaped nanoparticle through a dynamic multiscale model is crucial to provide biological insights on the transportation and adhesion mechanisms.

* To whom correspondence should be addressed. Address: Department of Mechanical And Aerospace Engineering, The University of Texas at Arlington, TX 76019. Telephone: 817-272-1256. E-mail: yaling.liu@uta.edu

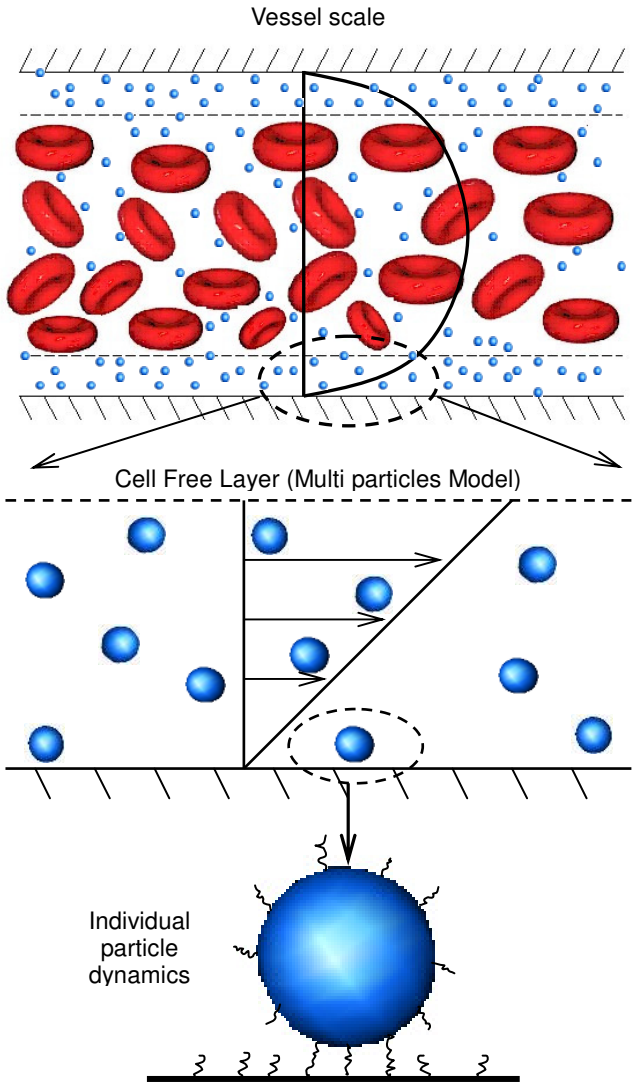

Fig. 1 Multiscale model of the targeted drug delivery

This paper presents for the first time, the simulation result for dynamic transportation and adhesion of non-spherical nanoparticles to vascular wall under shear flow using Brownian dynamics method coupled with adhesion kinetics model by the Immersed Finite Element Method (IFEM) platform[30-32]. In what follows, the adhesion kinetics of ligand-receptor binding interaction is described first. The nanoparticle Brownian dynamics is then coupled with the adhesion kinetics to describe motion of nanoparticle under vascular flow conditions. It is known that to initiate bond formation, nanoparticles must stay very close to the wall surface, inside a near-wall region known as cell free layer (CFL)[33], as shown in Fig. 1. The red blood cells flow with relatively higher velocity in the core region of vessel, leaving a pure plasma region with lower velocity close to vessel wall. The existence of CFL makes it reasonable to only consider nanoparticles in deposition process. The thickness of the cell free layer is found to be varying from 2-5 μm, independent of vessel size for vessels with diameter above 20 μm [34-36]. This suggests that binding probabilities of nanoparticles should be studied for a range of CFL thicknesses. In the following sections of this paper, the nanoparticle adhesion kinetics theory and modeling method are described first. Then, adhesion processes and trajectories for nanoparticles of different shapes and ligand densities are presented. Next, the binding probability of nanoparticles for a range of CFL thicknesses is studied. Finally, the conclusion and future work are presented.

Nanoparticle Adhesion Kinetics

To achieve targeted drug delivery, nanoparticles are usually coated with polymers that bind specifically to a particular type of receptors on the vessel cell surface [37]. The ligand-receptor binding will be coupled with Brownian dynamics with the IFEM platform. IFEM can be used for fully

coupled fluid-structure interaction problems, i.e., solving particle motion in a fluid while capturing the influence of particle on fluid flow. However, due to Brownian motion, it is computationally expensive to calculate the change of fluid flow due to particle motion at every time step. Since effect of nanoparticle motion is limited locally, we neglect the influence of particle motion on the fluid flow and focus on the particle motion and the adhesion process. Moreover, although IFEM can handle deformable particles immersed in a fluid, the nanoparticles are treated as rigid bodies in this work since our focus is on particle shape effect on adhesion process. The particle compliance will be the topic of future studies.

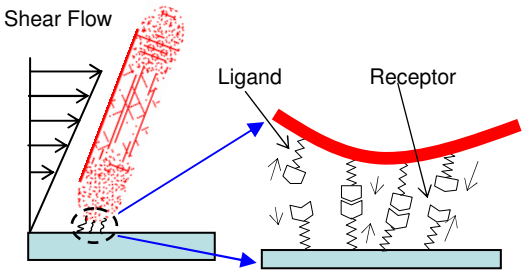

Figure.2. Model of ligand-receptor binding dynamics between particle surface and receptor coated surface.

The ligand-receptor binding is described as a non-covalent interaction process. When a particle approaches the vascular wall, ligands on the particle surface form non-covalent bonds with receptors on the vascular wall, as demonstrated in Fig. 2. An adhesion kinetic equation is used to calculate the bond density N_b [38]:

$$\frac{\partial N_b}{\partial t} = k_f (N_l - N_b)(N_r - N_b) - k_r N_b \quad (1)$$

Where, N_l and N_r are the ligand and receptor densities; k_r and k_f are the reverse and forward reaction rates, respectively. This interaction model represents a conservation equation of the different species (ligands, receptors, and bonds). The k_r and k_f are a function of bond length:

$$k_r = k_r^0 \exp\left(-(k_s - k_{ts})L^2 / 2B_z\right) \quad (2)$$

$$k_f = k_f^0 \exp\left(-k_{ts} L^2 / 2B_z\right) \quad (3)$$

Where k_s is the bond elastic constant; k_{ts} is the bond elastic constant at transient state; B_z is thermal energy; k_r^0 and k_f^0 are the reverse and forward reaction rates at zero load of ligand-receptor pair, respectively; L is the difference of bond length y and equilibrium length λ. The receptor-ligand bonds are modeled as springs with spring constant σ and equilibrium length λ, thus the bond forces are described as a function of bond length, y. Then, the ligand-receptor interaction forces can be summed on finite element surface through integration over the nanoparticle surface. Equations of bond forces and integrated adhesion forces are given as:

$$f_L = \sigma(y - \lambda) \quad (4)$$

$$\sigma^S \cdot n = \int N_b \, f_L(X^c) \, d\Gamma \quad (5)$$

Such adhesion force is coupled with the fluid-structure interaction force in the IFEM formulation. Similar adhesion model has been used by Chang et al. [39] and Dong et al. [40] in the study of white blood cell rolling. Besides the adhesion force, the Brownian force acting on to the nanoparticles is also important and is integrated into the IFEM formulation by adding a Brownian force term. The physical parameters used in the model are listed in Table 1 below.

Table 1. List of physical parameters used in the nanoparticle adhesion kinetics model

Definition	Symbol	Value	Reference
Ligand Density	N_l	2.0 x 10^{10} (sites/cm^2)	Lawrence and Springer (1991)[41]
Receptor Density	N_r	2.0 -5.0 x 10^{10} (sites/cm^2)	Bell et al. (1984)[42]
Reverse reaction rate	k_r	0.5 (1/s)	Bell (1978)[43]
Forward reaction rate	k_f	1.0 x 10^{-9} (cm^2/s)	Bell (1978) [43]
Equilibrium bond length	λ	20 nm	Bell (1978)[43]
Static bond spring constant	σ	0.5 (dyne/cm)	Dembo et al. (1988)[38]
Transient bond elastic constant	k_{ts}	0.48 (dyne/cm)	Dembo et al. (1988)[38]
Thermal Energy	B_z	4.0 x 10^{-14} (erg)	Dembo et al. (1988)[38]
Fluid viscosity	μ	0.01 (g/cm-s)	-

Nanoparticle Brownian Dynamics

Fundamental theories of Brownian dynamics indicates the impacts of random collisions from surrounding liquid molecules on motion of an immersed small particle.[44-46] The influence of Brownian motion on behavior of platelets and blood cells in blood flow has been studied extensively[2,47,48]. Patankar et al.[49] have proposed an algorithm for direct numerical simulation of Brownian motion by adding random disturbance in fluids. At microscale, the drag force acting on particles such as blood cells is significantly large (> 50 pN for particle size > 1 μm), thus Brownian motion is neglectable[47]. While at nanoscale, Brownian force becomes a dominant force to drive nanoparticle near vascular wall surface. And the drag force acting on a nanoparticle is relatively small. The random forces $\mathbf{R}(t)$ and torque $\mathbf{T}(t)$ acting on a nanoparticle is responsible for Brownian motion and rotation and satisfy the fluctuation-dissipation theorem[50]:

$$\langle \mathbf{R}_i(t) \rangle = 0 , \langle \mathbf{T}_i(t) \rangle = 0 \qquad (6)$$

$$\langle \mathbf{R}_i(t)\mathbf{R}_j(t') \rangle = 2\, k_B T \beta_t \delta_{ij}\, \delta(t-t')\boldsymbol{\delta}$$

$$\langle \mathbf{T}_i(t)\mathbf{T}_j(t') \rangle = 2\, k_B T \beta_r \delta_{ij}\, \delta(t-t')\boldsymbol{\delta} \qquad (7)$$

Where, $\boldsymbol{\delta}$ is the unit-second order tensor, δ_{ij} is the Kronecker delta, $\delta(t - t')$ is the Dirac delta function, k_BT is thermal energy of system, β_t and β_r are the translational and rotational friction coefficient of nanoparticle, respectively.

The friction coefficient depends on several physical parameters, such as fluid viscosity, size and shape of the nanoparticle. The friction coefficient for spherical-shaped particles can be easily derived from Stokes' law. However, there is no empirical formula available for friction coefficient of particles with complex shapes. In literature, there are empirical formulas for friction coefficients of oblate or rod-shaped particle[51-53], but those are limited to only few shapes and couple of orientations only. In a recent work by Loth[54], a new empirical formula is proposed to calculate friction coefficient for a non-spherical particle. Based on this formulation, friction coefficient of rod shaped particles in this work is derived using an angle factor. When particle moves along the fluid flow, the relative velocity of the particle can be divided into components in two directions: parallel to flow and perpendicular to flow, as shown in Fig. 3.

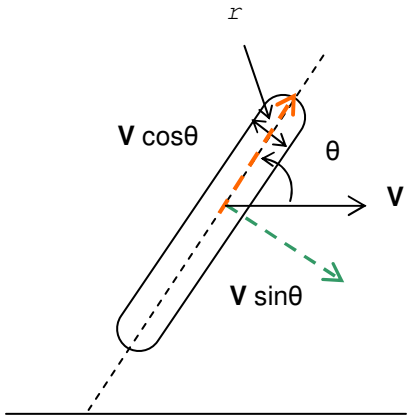

Fig. 3 Illustration of friction coefficient measurement of arbitrarily orientated nanorod

The friction coefficient of a rod shaped particle for an arbitrary orientation is given by [54]:

$$\beta_t = 3\pi\mu d_{equ} \times (f_{\parallel} \cdot |\cos\theta| + f_{\perp} \cdot |\sin\theta|) \qquad (8)$$

$$\beta_r = \pi\mu d^3_{equ} \qquad (9)$$

Where, β_t is friction coefficient for translation motion, β_r is friction coefficient for rotation motion, μ is fluid viscosity, d_{equ} is diameter of particle volume equivalent sphere, θ is the angle between flow direction and the long axis of the particle, $f_{\parallel}$ and $f_{\perp}$ are stokes correction factors for a spheroid particle moving parallel and perpendicular to the flow, respectively. These correction factors are expressed as [54]:

$$f_{\parallel} = \left(\frac{4}{5} + \frac{\gamma}{5}\right)\gamma^{-1/3} \qquad (10)$$

$$f_{\perp} = \left(\frac{3}{5} + \frac{2\gamma}{5}\right)\gamma^{-1/3} \qquad (11)$$

Where, γ is an aspect ratio of the spheroid particle. The velocity of a particle moving under a deterministic force in a fluid with velocity V_f, is given by:

$$\mathbf{V}_s = \left(\frac{\mathbf{F}_{deter}}{\beta_t} + \mathbf{V}_f\right)(1 - e^{-\frac{b_t}{m}t}) \qquad (12)$$

Where, F_{deter} is the total deterministic forces acting on the nanoparticle (Brownian force, adhesion force, etc.), V_s and V_f are solid and fluid velocity vector, respectively. For a time step much greater than characteristic time constant (m/β_t), the nanoparticle moves with a terminal velocity and Eq. (12) reduces to:

$$\mathbf{V}_s = \frac{\mathbf{F}_{deter}}{\beta_t} + \mathbf{V}_f \qquad (13)$$

By implementing this approach, we assume that deterministic force acting on the particle is balanced by the drag force from the fluid. This is a reasonable assumption since the mass of a nanoparticle is so small that inertia effect can be neglected. This terminal velocity is then use to update the nanoparticle position in translation direction. Similarly, the angular velocity of nanoparticle can be obtained through:

$$\omega_s = \frac{T_{\det er}}{\beta_r} + \omega_f \quad (14)$$

Where, ω_f is the angular velocity due to fluid flow. Using this translational and angular velocity, particle nodal positions are updated based on its distance from the center of the particle as:

$$\mathbf{v_i} = \mathbf{V_s} + \omega \times \mathbf{r_i} \quad (15)$$

The fluid flow in our simulation is assumed to be an incompressible viscous fluid governed by the Navier–Stokes equations:

$$\rho\left(\frac{\partial \mathbf{v}_f}{\partial t} + \mathbf{v}_f \cdot \nabla \mathbf{v}_f\right) = -\nabla p + \mu \nabla^2 \mathbf{v}_f \quad (16)$$

$$\nabla \cdot \mathbf{v}_f = 0 \quad (17)$$

The Navier-Stokes equations are solved through finite element method. To reduce numerical oscillations, the velocity test function is employed along with the stabilization parameters. Using integration by parts and the divergence theorem, the Patrov-Galarkin weak form is obtained. Then, the non-linear system is solved using the Newton-Raphson method. Moreover, the Generalized Minimum Residual (GMRES) iterative algorithm is employed to improve computation efficiency and to compute residuals based on matrix-free techniques [55]. The details of the derivation and implementation can be referred to Zhang et. al. and Liu et.al [30-32].

Theoretical Model of Nanoparticle Dissociation Probability

A numerical model is built based on the previous work by Decuzzi and Ferrari [27,56] to describe the cell targeting processes of nanorods and nanospheres under flow conditions. The adhesion probability P_a is characterized by the probabilistic kinetic formulation of McQuarrie [57]:

$$P_a \simeq m_r m_l K_a^o A_c \exp\left[-\frac{\lambda f}{k_B T}\right] \quad (18)$$

Where, m_r is receptor density on the substrate surface, m_l is ligand density on particle surface, A_c is contact area of particle, f is force acting per unit ligand-receptor pair, k_BT is thermal energy of system, λ is a characteristic length of ligand-receptor bond, and K_a^o is the affinity constant of ligand-receptor pair at zero load. f can be expressed further by the following formula:

$$f = F_{dis}/A_c = F/A_c + 2T/(A_c r_o) \quad (19)$$

Where, F_{dis} is the dislodging force due to hydrodynamic forces, comprised of two components, drag force along the flow direction $F = 6\pi a l \mu S F^s$ and torque $T = 4\pi a^3 \mu S T^s$. The contact area of the particle A_c is a surface area of the spheroid below a separation distance h_o from the wall surface. It can be approximated as the following:

$$A_c \cong \pi r_o^2 = \pi a^2\left[1 - \left(1 - \frac{h_o - \delta_{eq}}{a}\gamma\right)^2\right] \quad (20)$$

Where, a is a major radius of the particle, δ_{eq} is an equilibrium separation distance between the particle and wall surface, and γ is an aspect ratio of the particle. The details of the formulation and the constants used in the model can be found in a reference [58].

Once the adhesion probability is derived from the equation of probabilistic formulation (Eq. 18), the dissociations probability (P_d) can be easily calculated as 1-P_a. The dissociation probability is normalized by dissociation probability at zero shear rates to limit the range from 0 to 1. The normalized dissociation probability (P_d) of nanorod and nanosphere under different shear rates is plotted in Fig. 4. In this study, nanosphere of 100 nm radius is considered, while nanorod of the same radius but with aspect ratio of 5 is considered.

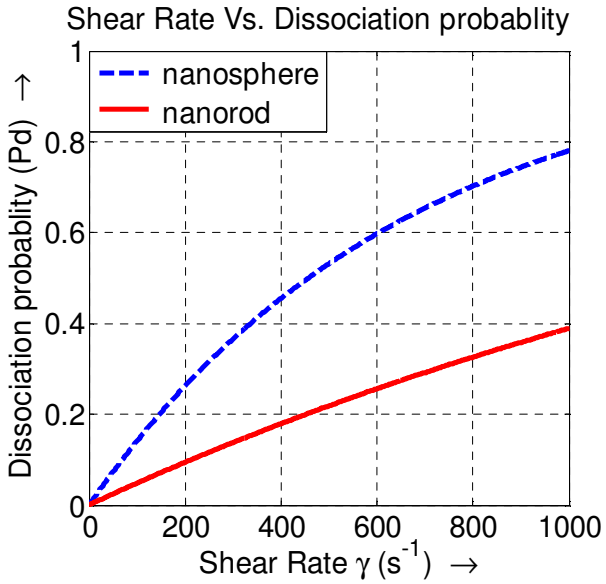

Fig. 4 Particle dissociation probabilities as a function of shear rate for nanorod and nanosphere. The dissociation probability is normalized with zero shear rate of respective nanoparticle.

As shown in Fig.4, increase in shear rate induces larger shear/dislodging force; thus increases the dissociation probability of nanoparticles. For a given shear rate, the dissociation probability of a nanorod is significantly less than that of a nanosphere, since the nanorod has larger surface area available for bond formation. While an analytical expression can be derived for the dissociation probability of nanosphere or nanorod, the binding probability is much more complex and needs to be obtained numerically due to the dynamic binding process, where the configuration of nanoparticle changes under deterministic forces. The significance of the binding probability is discussed in later sections.

Simulation Results

There are numerous physical factors that impact nanoparticle interaction with a surface under shear flow, such as particle-wall distance, particle shape, shear rate etc. In particular, the influences of particle shape and ligand density on adhesion will be the focus of this paper. The mesh

information, the nanoparticles and channel dimensions are mentioned in supplemental information section.

Influence of Nanoparticle Shape on Adhesion Kinetics

To test the influence of nanoparticle shape on adhesion kinetics, two nanoparticles of different shapes, spherical and non–spherical, but of the same volumes are considered. The simulations are carried over the channel with a length of 5 µm and a height of 2 µm. The length of rod shaped particle is 1000 nm and aspect ratio is 5. The diameter of spherical particle is 380 nm. In the simulation, a spherical particle and rod-shaped particle are initially positioned with their center 600 nm above a receptor-coated surface, as shown in Fig. 5.

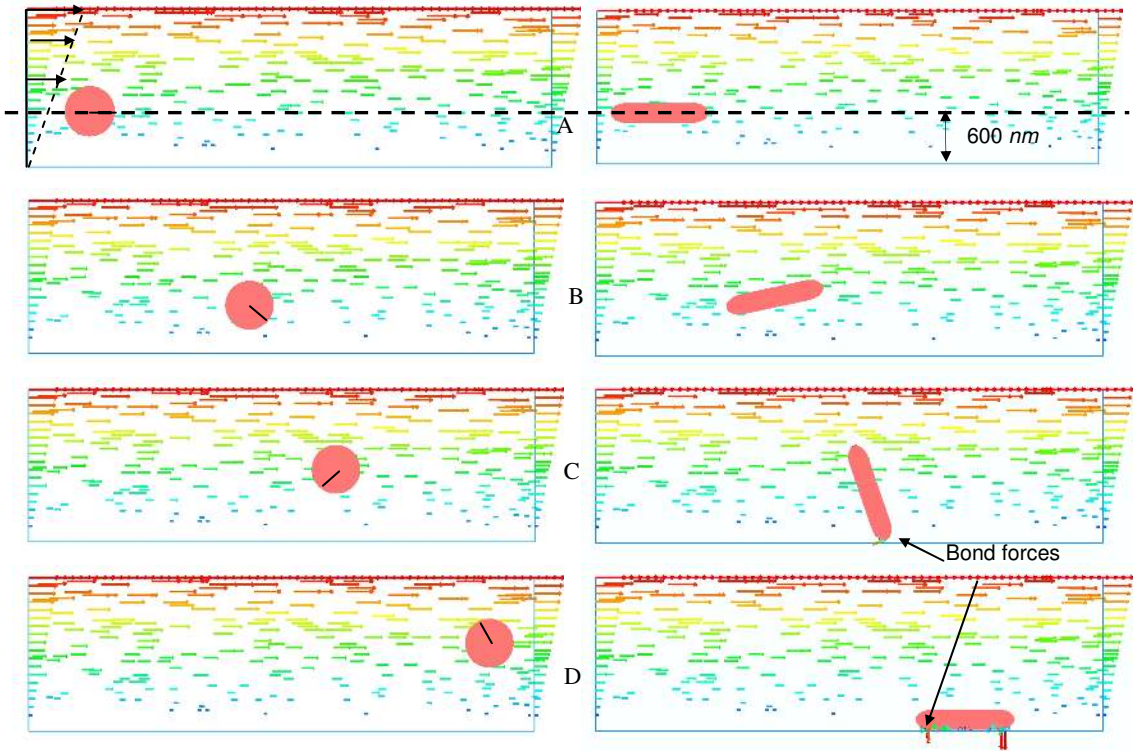

Fig.5. Shape dependent adhesion dynamics. The left column shows a spherical particle washed away without contact with surface; the right column shows nanorod tumbles and gets deposited. A, B, C, D are at time t=0 s, 0.25 s, 0.5s, and 0.75 s, respectively. The line on the spherical particle indicates its rotation. The vectors in fluid domain indicates flow field and arrows indicates magnitude and direction of bonding forces.

The shear velocity is applied at the top of channel to generate a shear rate of $8.0s^{-1}$ as shown in Fig. 5. Nanoparticles are allowed to move freely through the channel under influence of shear flow and Brownian force. For the case demonstrated in Fig.5, the spherical particle fails to make any contact or interaction with the vessel wall while it travels through the channel. Although Brownian motion is incorporated in the model, but for the given velocity and a channel length, Brownian diffusion isn't large enough to make the spherical particle to reach close enough to the wall surface, required to initialize bonding. Due to the non-spherical shape, rod-shaped particle exhibits tumbling motion while flowing through the channel. Due to the tumbling motion, the rod-shaped particle contacts with the receptor coated wall with bonds formed at the long axis end first. Then under steadily growing adhesion force, nanoparticle firmly adheres to the vessel wall and settles at its equilibrium state. Though the simulation result is just for one trial and doesn't provide any quantitative data, but it is able to differentiate the adhesion process of nanoparticles of two different shapes.

Influence of Ligand Density on Adhesion Kinetics

Besides the shape, ligand density also largely influences nanoparticle adhesion kinetics. To investigate the effect of ligand density on nanoparticle adhesion kinetics, the deposition process of two nanorods is compared under same physical flow condition.

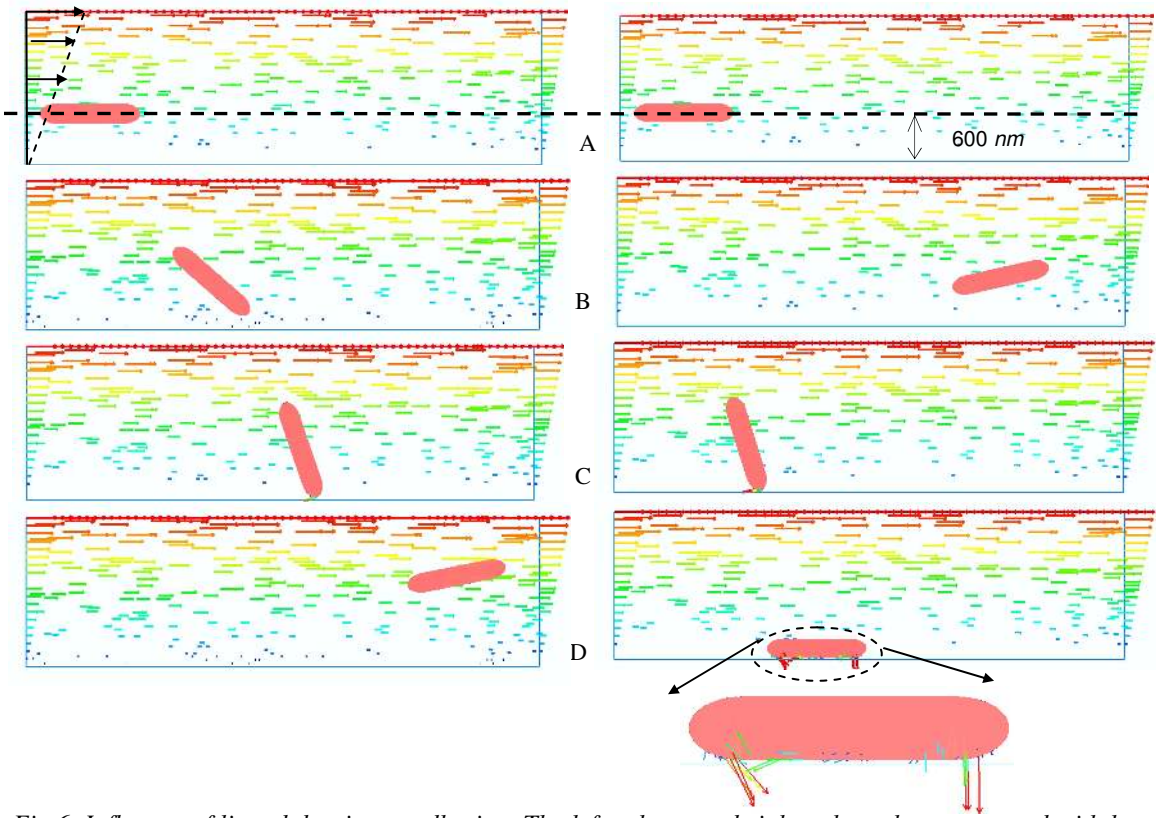

Fig.6. Influence of ligand density on adhesion. The left column and right column has a nanorod with low and high ligand coating respectively; A, B, C, D are at t=0 s, 0.25 s, 0.5s, and 0.75 s. The vectors in fluid domain indicates flow field and arrows indicates magnitude and direction of bonding forces.

Again, a shear rate of $8.0s^{-1}$ is generated within the channel, as shown in Fig. 6. Nanorods are coated with a ligand density of $410\mu m^{-2}$ and $3400\mu m^{-2}$, respectively. The corresponding number of ligands on each particle is 15 and 120, respectively. The significance of ligand density is that larger density results in stronger/faster bond formation. As shown in Fig. 6, the nanorod with low ligand density contacts with the wall surface at its end during tumbling motion, still it gets unbounded due to weak adhesion force. Thus, the limited numbers of ligands on the surface are unable to hold the nanoparticle at the contact site. In comparison, the nanorod with high ligand density firmly adheres upon initial contact as a result of multivalent bond formation. Therefore, the large number of bond sites ensures firm adhesion of nanorod at the contact site.

Trajectories of multiple nanoparticles

Nanorods are expected to have a higher probability to contact with the wall surface than their spherical counter parts because of tumbling motion. To test this hypothesis quantitively, trajectories of spherical and non-spherical nanoparticles under the same flow condition are compared. A shear rate of $8.0s^{-1}$ is generated at top of the channel. The simulations are carried over the channel with a length of 12 µm and a height of 1.5 µm.

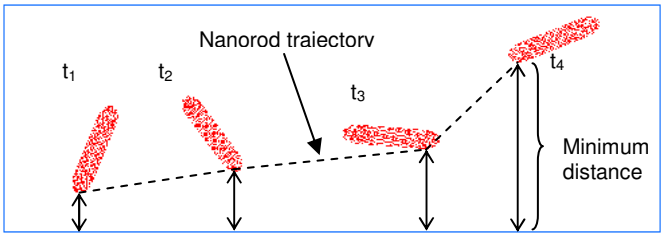

Fig.7. Illustration of measurement of minimum distance between a nanorod and the wall surface at different times

To illustrate the fluctuations of nanoparticle-wall distance, minimum distance between the nanoparticle and the wall surface is recorded over time, as illustrated in Fig. 7. Such trajectory indicates the contact-path of a nanoparticle when it flows through the channel. This determines how close the nanoparticle travels near the wall surface, which indeed dictates the binding events of the nanoparticle.

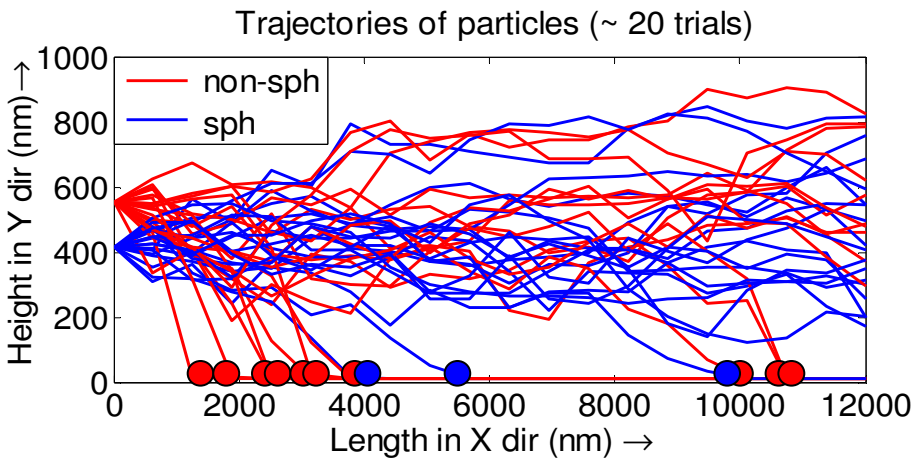

A

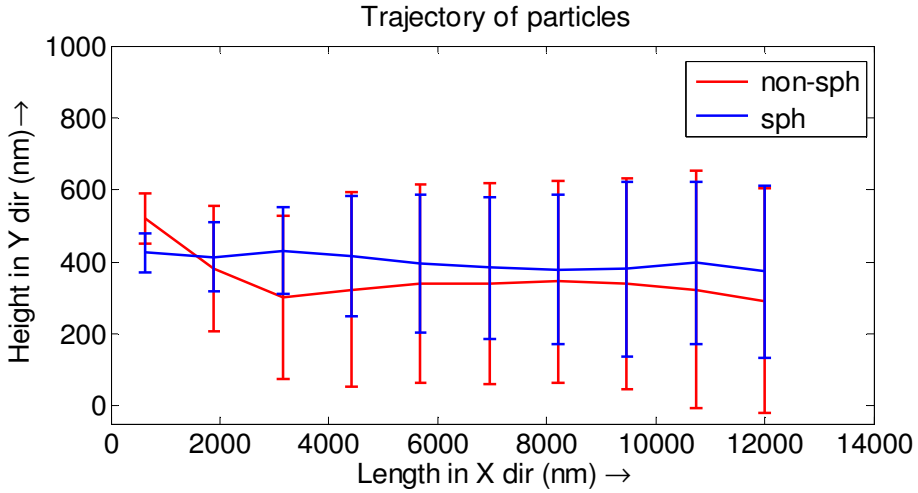

B

Fig.8. Comparing trajectories of nanorod and spherical particles to study shape effect on particle adhesion dynamics (a) Trajectories of 20 trials of nanorod and nanosphere, where red spot indicates adhesion of nanorod and blue spot indicates adhesion of nanosphere at that location (b) Mean trajectory of 20 trials of nanorod and nanosphere with standard deviation shown as vertical bar.

In a series of runs, a nanosphere and a nanorod are placed initially 650 nm above the wall surface. The trajectories of nanorod and nanosphere in twenty independent simulations are plotted in Fig. 8 (A). The simulation result elucidates that a nanorod has larger fluctuations in trajectories due to tumbling motion, thus it has more contact/adhesion events compared to that of nanosphere, as shown in Fig. 8 (B). Moreover, out of twenty trials, ten nanorods are deposited while only three nanospheres are deposited. Probability of spherical particle to contact with wall surface is purely determined by limited Brownian diffusion; while in case of nanorod, probability of contact is enhanced by tumbling motion. Thus, this result supports hypothesis of this work that nanorod has higher contact probability than the nanosphere for given physical condition.

Binding probability of nanoparticles

The focus of this paper is to characterize the binding probability of nanoparticles under vascular conditions for a given depletion layer thickness. The theoretical model has shown that adhesion probability is influenced by several parameters such as ligand density, nanoparticle shape and size, vascular flow condition, etc. The effect of ligand density on nanoparticle adhesion dynamics is already been shown qualitatively in Fig. 6. However, the actual targeting process is a dynamic process, involving transportation and diffusion process. This suggests the need of another parameter namely, binding probability, which effectively represents the binding probability of nanoparticle from a certain distance of the wall surface. It is the binding probability that actually dictates how many nanoparticles will actually bind to the surface among the number of nanoparticles present within the cell free zone. This study is dedicated on studying the effect of two parameters, the channel height and the shear rate, on nanoparticle binding probability. To ensure consistency and to study sole effect of

mentioned parameters among all the cases, the rest of the parameters are kept constant. For example, the value of ligand density is assumed to be sufficiently high to guarantee firm adhesion of nanoparticles (typically, adhesion force varies from 1 pN – 100 pN, while dislodging forces are limited 0.01 pN). Moreover, in a recent study, it has been shown that once nanoparticle tether to the receptor coated surface, it is very unlikely that nanoparticle gets detached under hydrodynamics force [59]. As a consequence this section is focusing on determining binding probability of nanoparticles rather than adhesion probability. The simulation parameters are listed in table. 1, unless otherwise noted. The diameter and length of nanorod is 200 nm and 1000 nm, respectively. The diameter of nanosphere is 380 nm.

The simulation begins with randomly assigned initial positions of nanoparticle at the channel inlet and shear flow is applied in the channel. The nanoparticle transportation is described by Brownian adhesion dynamics model. To ensure statistical accuracy, binding probability is evaluated based on the results of ~ 200 independent trials. As described in introduction section, this study is focused on determining binding probability of nanoparticles within a special zone of interest known as cell-free layer (CFL) or depletion layer. The number of bonded nanoparticles is counted and normalized by the total number of nanoparticles to obtain the binding probability for a given cell-free layer (CFL) thickness under a given flow condition.

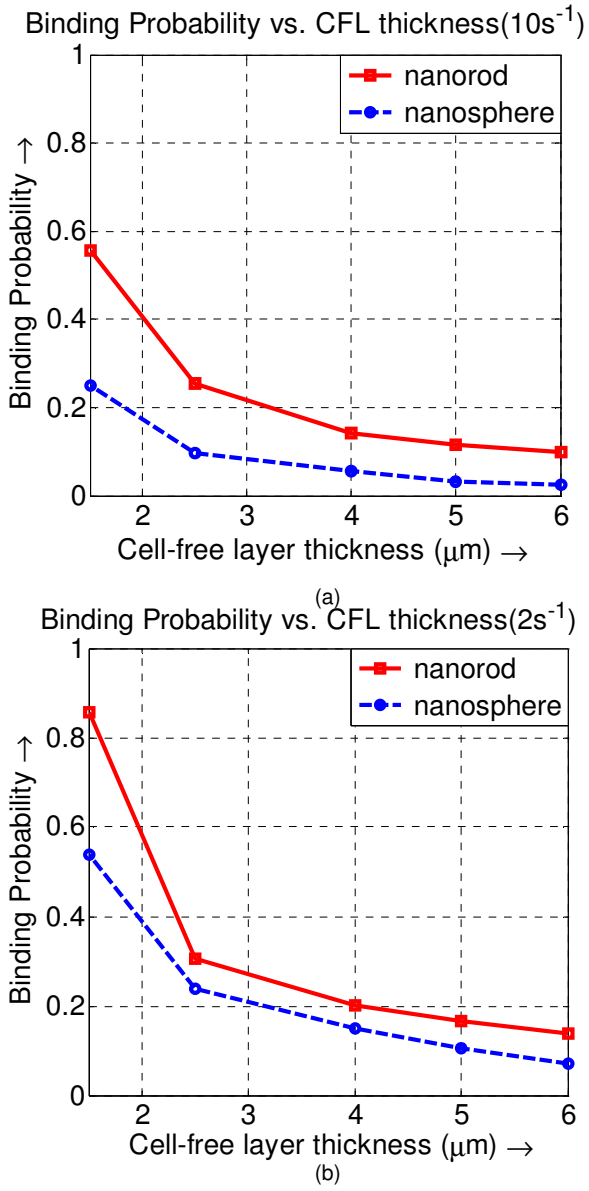

Fig.9. Studying effect of CFL thickness on binding probability of nanorods and nanosphere. (a) For shear rate of $2s^{-1}$, binding probability of nanorod and nanosphere is shown. (b) For shear rate of $10s^{-1}$, binding probability of nanorod and nanosphere is shown.

Binding probability of nanoparticles as a function of CFL thickness is plotted in Fig. 9 for two different shear rates, $2s^{-1}$ and $10s^{-1}$. The simulation result indicates that the nanorod has considerably higher binding probability than that of the nanosphere at both shear rates. Fig. 9(a) shows the binding probability of nanoparticles under a shear rate of $10s^{-1}$. As the CFL thickness increases, binding probability of nanoparticle decreases. Furthermore, due to limited diffusion length the binding probability of a nanosphere decreases almost linearly with CFL thickness, except for very low CFL thickness of 1.5 µm. At this thickness, the size of nanoparticle becomes comparable to the thickness size, thus transportation of nanosphere becomes diffusion dominant and resulting in high deposition probability. While the binding probability of nanorod decreases almost quadratically, mainly due to the tumbling motion. Furthermore, this result indicates that for a smaller CFL thickness, nanorod has significantly higher binding probability than nanosphere. As shear rate decreases, binding probability for both particles increases, since the diffusion motion becomes a dominating factor that enhances the binding events. Moreover, the less difference between binding probability of nanorod and nanosphere is observed at a shear rate of $2s^{-1}$, as shown in Fig. 9(b). At lower shear rates Brownian motion becomes a governing factor, and thus contribution of tumbling motion becomes marginal compare to the diffusion motion.

Besides shape, the effect of nanoparticle aspect ratio is investigated. Nanorods of two aspect ratios (5 and 10) are considered in the study and compared with nanospheres. Shear velocity is applied at the top of the channel and it is varied based on the shear rate of interest. It is found that nanoparticle with highest aspect ratio exhibit higher binding probability than that of other nanoparticles. The binding probability of nanoparticles under different shear rate is studied for a given CFL thickness of 5 µm. Binding probabilities as a function of shear rate for nanoparticles with three different aspect ratios are plotted in Fig.10. The simulation result elucidates that increase in shear rates reduces binding probability of nanoparticles, but the degree of reduction of binding probability varies with different nanoparticles. The simulation results imply that binding probability rapidly drops for nanosphere with increase in shear rate. While that of nanorods drops only marginally with increase in shear rate. This result clearly demonstrates advantage of nanorod over nanosphere in terms of binding probability over a range of shear rates.

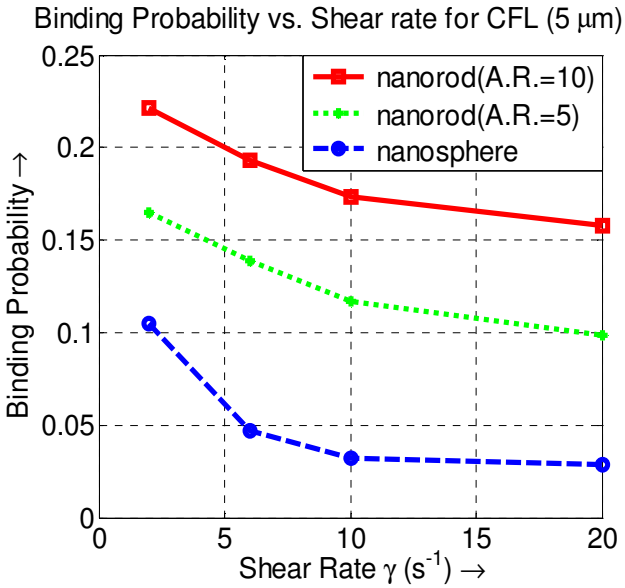

Fig.10. Studying effect of aspect ratio of nanoparticle on binding probability. Binding probability of nanorod and nanosphere under different shear rates for CFL thickness of 5 µm is shown.

Fig. 10 also shows that nanorod with higher aspect ratio has higher binding probability than that with lower aspect ratio. Binding probability of nanorod with higher aspect ratio is boosted by much larger tumbling motion. To summarize, the nanoparticle with larger aspect ratio has high binding probability and its binding probability decays slower with shear rate compared to that with low aspect ratio.

Conclusions

In summary, the adhesion kinetics of non-spherical nanoparticles is studied for the first time with hydrodynamics coupled with Brownian dynamics. The adhesion dynamics of nanoparticles are found to be influenced by the local flow shear rate, shapes, and ligand densities of the nanoparticle. To our knowledge, there does not exist another simulation method that can produce the results (Figs. 5, 6, 8, and 7) presented in this paper. While our focus here has been on the rod-shaped nanoparticles, this method is applicable to adhesion dynamics of arbitrarily-shaped nanoparticles. Binding probability of nanorods and nanospheres is determined for a range of Cell-free-layer thicknesses. It is found that nanorod has considerably higher binding probability compare to nanosphere under the same flow condition, mainly due to the tumbling motion. Moreover, with increase in shear rate, larger difference in adhesion probability between nanorod and nanosphere is found. Such knowledge can be used to optimize the design of shape and size of nanoparticle for desired nanomedicine function, and might eventually help shorten nano-carriers design cycles.

In the future, a more comprehensive model will be developed to include blood cells into the analysis since cell-particle interaction might influence the nanoparticle dispersion. This model will determine the coefficient called as dispersion coefficient, a parameter governing particles margination from main stream toward wall surface. Once that is achieved, it would be combined with the deposition rate at near wall region to get predict targeted drug delivery efficiency.

Acknowledgement

Y. Liu acknowledges the support of this work from University of Texas at Arlington Research Enhancement Program and National Institute of Health.

References

(1) Chauvierre, C.; Labarre, D.; Couvreur, P.; Vauthier, C. *Pharmaceutical Research* **2003**, *20*, 1786.

(2) Longest, P. W.; Kleinstreuer, C. *Journal of Biomechanics* **2003**, *36*, 421.

(3) Farokhzad, O. C.; Langer, R. *Advanced Drug Delivery Reviews* **2006**, *58*, 1456.

(4) Mathiowitz, E.; Jacob, J. S.; Jong, Y. S.; Carino, G. P.; Chickering, D. E.; Chaturvedi, P.; Santos, C. A.; Vijayaraghavan, K.; Montgomery, S.; Bassett, M.; Morrell, C. *Nature* **1997**, *386*, 410.

(5) Nasongkla, N.; Bey, E.; Ren, J. M.; Ai, H.; Khemtong, C.; Guthi, J. S.; Chin, S. F.; Sherry, A. D.; Boothman, D. A.; Gao, J. M. *Nano Letters* **2006**, *6*, 2427.

(6) Peppas, N. A. *Mrs Bulletin* **2006**, *31*, 888.

(7) Roney, C.; Kulkarni, P.; Arora, V.; Antich, P.; Bonte, F.; Wu, A. M.; Mallikarjuana, N. N.; Manohar, S.; Liang, H. F.; Kulkarni, A. R.; Sung, H. W.; Sairam, M.; Aminabhavi, T. M. *Journal of Controlled Release* **2005**, *108*, 193.

(8) Shah, P. *Mrs Bulletin* **2006**, *31*, 894.

(9) Sukhorukov, G. B.; Mohwald, H. *Trends in Biotechnology* **2007**, *25*, 93.

(10) Liu, Y.; Lu, W. L.; Zhang, Q. *Zhongguo Yi Xue Ke Xue Yuan Xue Bao* **2006**, *28*, 583.

(11) Sharma, G.; Anabousi, S.; Ehrhardt, C.; Ravi Kumar, M. N. *J Drug Target* **2006**, *14*, 301.

(12) Maysinger, D.; Lovric, J.; Eisenberg, A.; Savic, R. *Eur J Pharm Biopharm* **2007**, *65*, 270.

(13) Sutton, D.; Nasongkla, N.; Blanco, E.; Gao, J. *Pharm Res* **2007**, *24*, 1029.

(14) Torchilin, V. P. *Cell Mol Life Sci* **2004**, *61*, 2549.

(15) Gao, X.; Yang, L.; Petros, J. A.; Marshall, F. F.; Simons, J. W.; Nie, S. *Curr Opin Biotechnol* **2005**, *16*, 63.

(16) Smith, A. M.; Ruan, G.; Rhyner, M. N.; Nie, S. *Ann Biomed Eng* **2006**, *34*, 3.

(17) Koenig, S.; Chechik, V. *Langmuir* **2006**, *22*, 5168.

(18) Lou, X.; Wang, C.; He, L. *Biomacromolecules* **2007**, *8*, 1385.

(19) Yang, Y.; Nogami, M.; Shi, J.; Ruan, M. *J Nanosci Nanotechnol* **2005**, *5*, 179.

(20) Cheng, Y.; Gao, Y.; Rao, T.; Li, Y.; Xu, T. *Comb Chem High Throughput Screen* **2007**, *10*, 336.

(21) Duncan, R.; Izzo, L. *Adv Drug Deliv Rev* **2005**, *57*, 2215.

(22) Najlah, M.; D'Emanuele, A. *Curr Opin Pharmacol* **2006**, *6*, 522.

(23) Geng, Y.; Dalhaimer, P.; Cai, S. S.; Tsai, R.; Tewari, M.; Minko, T.; Discher, D. E. *Nature Nanotechnology* **2007**, *2*, 249.

(24) Liu, Z.; Cai, W. B.; He, L. N.; Nakayama, N.; Chen, K.; Sun, X. M.; Chen, X. Y.; Dai, H. J. *Nature Nanotechnology* **2007**, *2*, 47.

(25) Park, J. H.; von Maltzahn, G.; Zhang, L. L.; Schwartz, M. P.; Ruoslahti, E.; Bhatia, S. N.; Sailor, M. J. *Advanced Materials* **2008**, *20*, 1630.

(26) Galbraith, C. G.; Sheetz, M. P. *Current Opinion in Cell Biology* **1998**, *10*, 566.

(27) Decuzzi, P.; Ferrari, M. *Biomaterials* **2006**, *27*, 5307.

(28) Decuzzi, P.; Lee, S.; Bhushan, B.; Ferrari, M. *Annals of Biomedical Engineering* **2005**, *33*, 179.

(29) Decuzzi, P.; Lee, S.; Decuzzi, M.; Ferrari, M. *Annals of Biomedical Engineering* **2004**, *32*, 793.

(30) Zhang, L.; Gerstenberger, A.; Wang, X. D.; Liu, W. K. *Computer Methods in Applied Mechanics and Engineering* **2004**, *193*, 2051.

(31) Liu, W. K.; Liu, Y. L.; Farrell, D.; Zhang, L.; Wang, X. S.; Fukui, Y.; Patankar, N.; Zhang, Y. J.; Bajaj, C.; Lee, J.; Hong, J. H.; Chen, X. Y.; Hsu, H. Y. *Computer Methods in Applied Mechanics and Engineering* **2006**, *195*, 1722.

(32) Liu, W. K.; Kim, D. W.; Tang, S. Q. *Computational Mechanics* **2007**, *39*, 211.
(33) Zhang, J. F.; Johnson, P. C.; Popel, A. S. *Microvascular Research* **2009**, *77*, 265.
(34) Woodcock, J. P. *Reports on Progress in Physics* **1976**, *39*, 65.
(35) Bayliss, L. E. *J Physiol* **1959**, *149*, 593.
(36) Taylor, M. *Aust J Exp Biol Med Sci* **1955**, *33*, 1.
(37) Lutters, B. C. H.; Leeuwenburgh, M. A.; Appeldoorn, C. C. M.; Molenaar, T. J. M.; Van Berkel, T. J. C.; Biessen, E. A. L. *Current Opinion in Lipidology* **2004**, *15*, 545.
(38) Dembo, M.; Torney, D. C.; Saxman, K.; Hammer, D. *Proceedings of the Royal Society of London Series B-Biological Sciences* **1988**, *234*, 55.
(39) Chang, K. C.; Tees, D. F. J.; Hammer, D. A. *Proceedings of the National Academy of Sciences of the United States of America* **2000**, *97*, 11262.
(40) Dong, C.; Cao, J.; Struble, E. J.; Lipowsky, H. W. *Annals of Biomedical Engineering* **1999**, *27*, 298.
(41) Lawrence, M. B.; Springer, T. A. *Cell* **1991**, *65*, 859.
(42) Bell, G. I.; Dembo, M.; Bongrand, P. *Biophysical Journal* **1984**, *45*, 1051.
(43) Bell, G. I. *Science* **1978**, *200*, 618.
(44) Einstein, A. *Investigations on the Theory of Brownian Movement*; New York: Dover, 1956.
(45) Ermak, D. L.; Mccammon, J. A. *Journal of Chemical Physics* **1978**, *69*, 1352.
(46) Li, A.; Ahmadi, G. *Aerosol Science and Technology* **1992**, *16*, 209.
(47) Mody, N. A.; King, M. R. *Langmuir* **2007**, *23*, 6321.
(48) Gentile, F.; Ferrari, M.; Decuzzi, P. *Annals of Biomedical Engineering* **2008**, *36*, 254.
(49) Sharma, N.; Patankar, N. A. *Journal of Computational Physics* **2004**, *201*, 466.
(50) Mori, N.; Kumagae, M.; Nakamura, K. *Rheologica Acta* **1998**, *37*, 151.
(51) Inthavong, K.; Wen, H.; Tian, Z. F.; Tu, J. Y. *Journal of Aerosol Science* **2008**, *39*, 253.
(52) Haider, A.; Levenspiel, O. *Powder Technology* **1989**, *58*, 63.
(53) Tran-Cong, S.; Gay, M.; Michaelides, E. E. *Powder Technology* **2004**, *139*, 21.
(54) Loth, E. *Powder Technology* **2008**, *182*, 342.
(55) Saad, Y.; Schultz, M. H. *Siam Journal on Scientific and Statistical Computing* **1986**, *7*, 856.
(56) Decuzzi, P.; Ferrari, M. *Biomaterials* **2008**, *29*, 377.
(57) McQuarrie, D. A. *Journal of Chemical Physics* **1963**, *38*, 433.
(58) Decuzzi, P.; Ferrari, M. *Biomaterials* **2006**, *27*, 5307.
(59) Haun, J. B.; Hammer, D. A. *Langmuir* **2008**, *24*, 8821.